RESEARCH ARTICLE

# Multimodal Magnetic Resonance Imaging Quantification of Brain Changes in Progressive Supranuclear Palsy

Nadya Pyatigorskaya, MD, PhD,[1,2,3*] Lydia Yahia-Cherif, PhD,[1,2] Rahul Gaurav,[1,2] Claire Ewenczyk, MD, PhD,[2,4] Cecile Gallea, PhD,[1,2] Romain Valabregue, PhD,[1,2] Fatma Gargouri, PhD,[1,2] Benoit Magnin, MD,[5] Bertrand Degos, MD, PhD,[6] Emmanuel Roze, MD, PhD,[2,4] Eric Bardinet, PhD,[1,2] Cyril Poupon, PhD,[7] Isabelle Arnulf, MD, PhD,[2,8] Marie Vidailhet, MD, PhD,[2,4] and Stéphane Lehericy, MD, PhD[1,2,3]

[1]*Institut du Cerveau et de la Moelle–ICM, Centre de NeuroImagerie de Recherche–CENIR, Paris, France*
[2]*ICM, Sorbonne Université, UPMC Univ Paris 06, UMR S 1127, CNRS UMR 7225, Paris, France*
[3]*Service de Neuroradiologie, APHP, Hôpital Pitié-Salpêtrière, Paris, France*
[4]*Clinique des mouvements anormaux, Département des Maladies du Système Nerveux, Hôpital Pitié-Salpêtrière, APHP, Paris, France*
[5]*Service de Radiologie, CHU Clermont-Ferrand, Clermont-Ferrand, France*
[6]*Service de Neurologie, Hôpital Avicenne, APHP, Bobigny, France*
[7]*NeuroSpin, CEA, Gif-Sur-Yvette, France*
[8]*Service de pathologies du Sommeil, Hôpital Pitié-Salpêtrière, APHP, Paris, France*

**ABSTRACT: Background:** Progressive supranuclear palsy (PSP) is a neurodegenerative clinically heterogeneous disorder, formal diagnosis being based on postmortem histological brain examination.

**Objective:** We aimed to perform a precise in vivo staging of neurodegeneration in PSP using quantitative multimodal MRI. The ability of MRI biomarkers to differentiate PSP from PD was also evaluated.

**Methods:** Eleven PSP patients were compared to 26 age-matched healthy controls and 51 PD patients. Images were acquired at 3 Tesla (three-dimensional $T_1$-weighted, diffusion tensor, and neuromelanin-sensitive images) and 7 Tesla (three-dimensional-$T_2$* images). Regions of interest included the cortical areas, hippocampus, amygdala, basal ganglia, basal forebrain, brainstem nuclei, dentate nucleus, and cerebellum. Volumes, mean diffusivity, and fractional anisotropy were measured. In each region, a threshold value for group categorization was calculated, and four grades of change (0–3) were determined.

**Results:** PSP patients showed extensive volume decreases and diffusion changes in the midbrain, SN, STN, globus pallidus, basal forebrain, locus coeruleus, pedunculopontine nucleus, and dentate nucleus, in close agreement with the degrees of impairment in histological analyses. The predictive factors for the separation of PSP and healthy controls were, in descending order, the neuromelanin-based SN volume; midbrain fractional anisotropy; volumes of the midbrain, globus pallidus, and putamen; and fractional anisotropy in the locus coeruleus. The best predictors for separating PSP from PD were the neuromelanin-based volume in the SN, fractional anisotropy in the pons, volumes of the midbrain and globus pallidus, and fractional anisotropy in the basal forebrain.

**Conclusions:** These results suggest that it is possible to evaluate brain neurodegeneration in PSP noninvasively, even in small brainstem nuclei, in close agreement with previously published histological data. © 2019 International Parkinson and Movement Disorder Society

**Key Words:** biomarkers; diffusion tensor imaging; movement disorders; PSP; volumetry

***Correspondence to:** Dr. Nadya Pyatigorskaya, CENIR, ICM, Hôpital Pitié-Salpêtrière 47-83 Boulevard de l'Hôpital, 75651 Paris Cedex 13, France; E-mail: nadya.pyatigorskaya@gmail.com

**Funding agencies:** This work was supported by grants from PSP France, Agence Nationale de la Recherche (ANRMNP 2009, Nucleipark), DHOS-Inserm (2010, Nucleipark), France Parkinson (2008), Ecole Neuroscience de Paris, the Investissements d'Avenir, IAIHU-06 (Paris Institute of Neurosciences–IHU), ANR-11-INBS-0006, Fondation d'Entreprise EDF, the Fondation Thérèse, and René Planiol pour l'étude du Cerveau.

**Relevant conflicts of interest/financial disclosures:** Marie Vidailhet received funding from PSP France, the Investissements d'Avenir, IAIHU-06 (Paris Institute of Neurosciences–IHU), ANR-11-INBS-0006, Fondation d'Entreprise EDF, the Fondation Thérèse, and René Planiol pour l'étude du Cerveau. Stéphane Lehericy received grants from "Investissements d'avenir" [grant numbers ANR-10-IAIHU-06 and ANR-11-INBS-0006] and Biogen Inc.

Full financial disclosures and author roles may be found in the online version of this article.

**Received:** 14 June 2019; **Revised:** 17 August 2019; **Accepted:** 15 September 2019

**Published online 11 November 2019 in Wiley Online Library (wileyonlinelibrary.com). DOI: 10.1002/mds.27877**

PSP is a heterogeneous neurodegenerative disease characterized by motor, behavioral, and cognitive disorders. The classical form of PSP is referred to as Richardson syndrome, but other variants have been described.[1-3] While the classical symptoms include a gradually progressive occurrence of vertical supranuclear gaze palsy and postural instability,[4,5] symptoms can be much less specific. The definite diagnosis of PSP is thus based on postmortem histological examination.

PSP is a tauopathy characterized by neurodegeneration in specific brain areas,[1,6,7] including the basal ganglia, the nucleus basalis of Meynert (NBM), nuclei in midbrain regions such as the SN, cuneiform nucleus, and pedunculopontine nucleus (PPN), and pons regions such as the locus coeruleus (LC) and, to a lesser degree, the medulla oblongata.[1,8]

Neuroimaging is useful to detect brain changes in PSP and facilitate disease diagnosis. The classical PSP MRI aspect includes a specific midbrain atrophy pattern,[9-11] with volumetric decrease, diffusion imaging, and relaxometry changes in the basal ganglia and midbrain.[12-14] These changes usually discriminate patients with PSP Richardson syndrome (PSP-RS) from those with Parkinson's disease (PD) and healthy controls (HCs), but this may not be the case for other PSP presentations.[15] A more precise characterization of PSP-related neurodegeneration in the small nuclei of the brainstem and basal forebrain using MRI may improve this discrimination.

Here, we used multimodal quantitative MRI to study the detailed distribution and extent of brain changes in the central nervous system, including the small brainstem nuclei, basal ganglia, basal forebrain, and cortical regions, relative to a previous seminal pathological study.[1] We also examined the biomarker combinations that were most efficient in differentiating PSP from PD patients and HCs.

# Subjects and Methods

## Subjects

Patients were prospectively recruited at the Movement Disorders Clinic of Pitie-Salpetriere Hospital between April 2010 and September 2012 in the frame of the Nucleipark study (ID-RCB 2009-A00922-55). Patients with PSP-RS were compared to age-matched HCs and PD patients. Inclusion criteria were as follows: (1) clinical diagnosis of idiopathic PD according to the UK Parkinson's Disease Society Brain Bank criteria, age ranging between 18 and 75 years, and Mini-Mental State Examination (MMSE) score > 24; (2) clinical diagnosis of PSP according to Litvan's National Institute of Neurological Disorders and Stroke (NINDS) criteria;[4] and (3) HCs were matched for age and sex and did not present any medical history of neurological disorders. PSP-RS patients also fulfilled the International Parkinson and Movement Disorder Society (MDS) criteria for possible PSP.[2] Exclusion criteria were contraindications to MRI or psychiatric disorders or any abnormalities on the MRI scan. All subjects gave written informed consent. The study was approved by the local ethics committee (internal review board of Paris VI).

## Clinical Examination

Motor disability was evaluated using the UPDRS-III, in the *off* condition (12-hour dopaminergic treatment withdrawal). The neuropsychological assessment included the MMSE.

## MRI Data Acquisition

MRI acquisition was performed on a 3 Tesla (T) TRIO TIM system (Siemens, Erlangen, Germany) using a 12-channel receive-only head coil and a 7T MAGNETOM system (Siemens) using an eight-channel head coil. The 3T protocol included three-dimensional (3D) $T_1$-weighted (T1-w) images, 3D T2-weighted (T2-w) images, and diffusion tensor imaging (DTI). The 3D T1-w scans were acquired using sagittal magnetization-prepared rapid gradient echo acquisition with the following parameters: repetition time (TR)/echo time (TE)/flip angle: 2300 ms/4.18 ms/9 degrees, inversion time: 900 ms, voxel size: $1 \times 1 \times 1$ mm$^3$, 1 average. Neuromelanin (NM)-sensitive images were acquired using two-dimensional (2D) axial turbo spin echo T1-w images with the following parameters: TR/TE/flip angle: 900 ms/15 ms/180 degrees, voxel size: $0.4 \times 0.4 \times 3$ mm$^3$, three averages. DTI parameters were as follows: TR/TE/flip angle: 14,000 ms/101 ms/90 degrees, voxel size: $1.7 \times 1.7 \times 1.7$ mm$^3$, b-value: 1500 s/mm$^2$, and 60 diffusion gradient directions. The 3D T2*-w high-resolution images were acquired at 7T with the following parameters: TR/TE/flip angle: 2180 ms/29.9 ms/65 degrees, field of view: 192 mm$^2$, voxel size: $0.5 \times 0.5 \times 0.5$ mm$^3$, 40 slices.

Both 3 and 7Tesla MRI examinations were performed within 1 month of each other.

## Image Analysis

Image processing and analysis were performed using in-house software written in MATLAB (The MathWorks, Inc., Natick, MA).

### *Regions of Interest*

Regions of interest (ROIs) included 17 cortical and subcortical structures that were representative of PSP pathology based on previous histological studies,[1,6] including cortical regions (prefrontal cortex, middle-anterior cingulate cortex, precentral cortex, superior parietal cortex, parieto-occipital cortex, hippocampus, amygdala, and

temporal cortex), supratentorial white matter, basal forebrain, basal ganglia (caudate nucleus, putamen, globus pallidus, STN, and SN), brainstem regions (midbrain, pons, and medulla oblongata), brainstem nuclei (LC, PPN, and cuneiform nucleus), dentate nucleus (DN), and cerebellar gray matter and white matter. Cortical, globus pallidus, putamen, thalamus, and brainstem regions (midbrain, pons, and medulla oblongata) were segmented automatically using FreeSurfer (http://freesurfer.net/; MGH, Boston, MA) software (Supporting Information Fig. S1).

SN segmentations were manually performed at 3T using NM-sensitive images and FreeSurfer software and at 7T using 3D T2* images and ITK Snap software (ITK-Snap, Philadelphia, PA) by one trained examiner who was blinded to the clinical statuses of the subjects. To evaluate the accuracy of segmentation for each setting, a second examiner performed the segmentations. For NM images, the contours of the SN were manually drawn around the area of high signal intensity as previously described.[16] For 7T T2*-w images, the SN was defined as the area of hypointensity ventral to the red nucleus and dorsal to the cerebral peduncle. The STN was also manually segmented using 7T images. The LC was segmented semiautomatically with in-house software as described previously.[17] The cuneiform nucleus and PPN were segmented semiautomatically using in-house software and the YeB atlas.[18] The DN was manually segmented as the area of low signal intensity on the 3D T2 images. For the basal forebrain, we used the normalized masks of the septal area/vertical limb of the diagonal band (Ch1–2) and the horizontal limb of the diagonal band/NBM (Ch3–4) as previously described.[19]

DTI preprocessing was performed using the FMRIB Software Library (FSL; v5.0; FMRIB, Oxford, UK). Motion and eddy currents were corrected using the eddycor function. Echo-planar deformations were corrected using field maps. Fractional anisotropy (FA) and diffusivity maps were computed with the DTIfit function for the entire volume. A nonlocal means filter was applied.

### Quantitative Analysis

The DTI, NM-sensitive, and T2-w images were coregistered to the 3D T1-w volume using the SPM coregister function. Volume, mean FA value, and mean diffusivity (MD) value were calculated in all other segmented ROIs.

For the SN, volumes of NM-based ROIs were calculated using in-house MATLAB algorithms (The MathWorks Inc.). The signal ratio was calculated by normalizing the mean signal of the SN in each slice to the signal in the background region, which was manually traced, including the tegmentum and superior cerebellar peduncle (SCP).[20]

For the LC, we calculated the signal-intensity ratio by normalizing the mean signal of the 10 connected voxels with the brightest intensity to the signal in the background region using in-house software.[17]

In addition, for comparison, we measured the midbrain surface, pons surface, middle cerebellar peduncle diameter, SCP diameter, midbrain to pons surface ratio, and Magnetic Resonance Parkinsonism Index (MRPI).

## Statistical Analysis

Statistical analyses were performed using R software (R Core development Team 2015).

### Missing Data Handling

The rate of missing data was <1% of the total observations. We used a multiple imputation technique to address the missing data problem. Missing values for a target variable were estimated using additive regression and bootstrapping. Five replicates of the data set were computed using bootstrapping to draw a random sample from the nonmissing values of the same variable and fit a flexible additive model to predict the missing values.

### Nonparametric Tests

As a first-pass filter, to determine the discriminant ROIs, the neuroimaging measures were compared between the groups using the Kruskal-Wallis test followed by the Mann-Whitney U test for pairwise comparisons. Differences were considered significant at $P$ values <0.05. Variables that did not show statistically significant differences between the groups were discarded.

### Staging Procedure

To determine the grade of change in each region, we calculated a categorization threshold value using a receiver operating characteristic (ROC) curve. Sensitivity and specificity of the cut-off points were estimated using the Youden index, the optimal threshold giving the best sensitivity and specificity and optimally separating HCs from patients. Categorization accuracy was calculated pairwise as the total number of subjects correctly classified among all classified subjects. Regions with a specificity, sensitivity, and area under the curve (AUC) >0.7 were kept for the analyses. For a better comparison with previous histological studies,[1,6] we defined four grades of change (0–3) that were associated with each subject/variable. Based on cut-off values and local extrema, the grades were computed as follows:

$$l_{ij} = \begin{cases} \begin{cases} 0 & , v_{ij} < c_i \\ |v_{ij} - c_i| / |max_i - c_i| / 3 & , v_{ij} \geq c_i \end{cases} + \begin{cases} 1 \ \ if\ modulo(|v_{ij} - c_i|,\ |max_i - c_i|) \neq 0 & , m_{ih} \leq m_{ip} \\ 0 \qquad Otherwise & \end{cases} \\ \begin{cases} 0 & , v_{ij} \geq c_i \\ |v_{ij} - c_i| / |min_i - c_i| / 3 & , v_{ij} < c_i \end{cases} + \begin{cases} 1 \ \ if\ modulo\ (|v_{ij} - c_i|,\ |min_i - c_i| \neq 0 & , m_{ih} > mi \\ 0 \qquad Otherwise & \end{cases} \end{cases}$$

where $l_{ij}$ and $v_{ij}$ are the grades and observation value of the $j^{th}$ individual for the $i^{th}$ variable, respectively; $c_i$, $max_i$, and $min_i$ are the cut-off, maximal, and minimal values, respectively, of the $i^{th}$ variable; and $m_{ih}$ and $m_{ip}$ are the mean values of the $i^{th}$ variable for the healthy and patient groups, respectively.

### *Multiple Factor Analysis*

To determine the underlying structure of the data, we used multiple factor analysis (MFA) as a data-driven exploratory technique. Variables describing the same brain regions were grouped together to form a set of blocks. MFA was then run on the blocks associated with a brain region (Supporting Information Table S1). As a first step, individual principal component analysis (PCA) was performed on each block, and the result was then normalized by the corresponding first Eigen value. The obtained matrices were then merged to form a global matrix, and a global PCA was performed. The individual observations were then projected onto the global space to determine the differences/similarities between the individual groups and the relationships between the brain regions.

### *Logistic Regression*

Logistic regression was run using the predictors derived from the MFA to determine the most significant variables contributing to the separation between PD, PSP, and HC subjects.

## Data Availability

The algorithms used for the analyses herein are available upon request.

# Results

## Demographic Data

Eleven patients with PSP-RS were included and compared to 51 patients with PD and 26 HCs (Table 1). The UPDRS-III *off* was higher in PSP and PD subjects than in HCs. There were no significant differences in the overall UPDRS-III *off* scores, akinesia, rigidity, or axial subscores between PD and PSP subjects, whereas the UPDRS tremor score was lower in PSP subjects than in the PD group. There were no significant differences in MMSE scores between groups.

## Region-Based Nonparametric Analysis

Patients with PSP-RS showed extensive changes predominantly in the midbrain, SN, STN, globus pallidus, LC, and PPN. Significant volume decreases ($P \leq 0.006$) in a number of brain structures were observed in patients with PSP-RS compared to those in the PD and HC groups (Supporting Information Tables S2 and S3; Supporting Information Fig. S2). In the basal ganglia, decreased volume was observed ($P \leq 0.003$) in the globus pallidus, putamen, STN, and caudate nucleus. The thalamus showed reduced volume and FA. A greater volume decrease was observed in the midbrain than in the pons and the medulla oblongata ($P \leq 0.001$), as expected, and FA was reduced in the first two regions ($P \leq 0.006$; Supporting Information Fig. S2). The SN was the most affected structure in the midbrain, as shown by a reduced NM-sensitive volume and FA ($P \leq 0.0001$). FA was also reduced ($P \leq 0.005$) in the PPN, LC, cuneiform nucleus, and DN.

## Categorization Accuracies for PSP Characterization

Several of these markers achieved a good-to-excellent categorization accuracy for differentiating PSP-RS and HC subjects (Table 2 and Supporting Information Table S4). Categorization accuracies >0.85 were observed for volumes of the globus pallidus, midbrain, and putamen and for the NM-sensitive volume, NM-sensitive signal, and FA in the SN. Several biomarkers also achieved good-to-excellent categorization accuracies for differentiating PSP-RS and PD subjects. The highest categorization accuracies (≥0.85) were observed for volumes of the putamen, globus pallidus, midbrain, entire brainstem, and NM-based SN as

**TABLE 1.** Demographic and clinical data overlap

| | HC | PSP | PD | P-value | U-test HC/PSP | U-test HC/PD | U-test PD/PSP |
|---|---|---|---|---|---|---|---|
| Demographic data | | | | | | | |
| No. of subjects | 26 | 11 | 51 | | | | |
| Males/females | 12/14 | 4/7 | 36/15 | 0.08 | | | |
| Age (years) | 60.8 ± 8.3 | 61.7 ± 7.8 | 60.1 ± 10.1 | 0.2 | | | |
| Disease duration (years) | — | 3.8 ± 1.5 | 8.7 ± 3.5 | **<0.001** | | | |
| Motor clinical data | | | | | | | |
| UPDRS-III (*off*; ondition) (0–108) | 0.8 ± 0.1 | 28.3 ± 9.6 | 31.2 ± 9.9 | **<0.001** | **<0.001** | **<0.001** | 0.34 |
| URDRS axial score | 0.2 ± 0.5 | 5.5 ± 2.9 | 4.3 ± 2.7 | **<0.001** | **<0.001** | **<0.001** | 0.17 |
| UPDRS tremor score | 0.1 ± 0.4 | 0.9 ± 1.6 | 4.1 ± 3.7 | **<0.001** | 0.13 | **<0.001** | **0.002** |
| UPDRS akinesia score | 0.3 ± 0.7 | 20.7 ± 7.4 | 16.1 ± 5.4 | **<0.001** | **<0.001** | **<0.001** | 0.12 |
| UPDRS rigidity score | 0.0 ± 0.0 | 6.6 ± 4.4 | 5.5 ± 2.2 | **<0.001** | **<0.001** | **<0.001** | 0.51 |
| Neuropsychological **tests** | | | | | | | |
| MMSE (0–30) | 28.7 ± 4.8 | 27.1 ± 2.2 | 27.8 ± 1.2 | **0.09** | | | |

Groups were compared using the chi-square or Kruskal-Wallis test followed by the post-hoc Mann-Whitney U test. Significant *P* values are indicated in bold.

**TABLE 2.** AUC and categorization accuracy to distinguish the three groups*

| | | PSP/HC | | PSP/PD | | PD/HC | |
|---|---|---|---|---|---|---|---|
| Region | | AUC | CA | AUC | CA | AUC | CA |
| Globus pallidus | Volume | 0.98 | 0.91 | 0.98 | 0.94 | 0.65 | 0.68 |
| Caudate nucleus | Volume | 0.85 | 0.74 | 0.78 | 0.64 | 0.55 | 0.54 |
| Putamen | Volume | 0.96 | 0.86 | 0.93 | 0.87 | 0.56 | 0.61 |
| STN | 7T volume | 0.89 | 0.83 | 0.82 | 0.79 | 0.58 | 0.57 |
| Thalamus | Volume | 0.81 | 0.73 | 0.86 | 0.73 | 0.62 | 0.57 |
| | FA | 0.84 | 0.82 | 0.88 | 0.85 | 0.54 | 0.5 |
| Ch3 to 4, NBM | FA | 0.94 | 0.91 | 0.93 | 0.83 | 0.51 | 0.51 |
| Ch1 to 2 | FA | 0.93 | 0.92 | | | 0.63 | 0.54 |
| Brainstem | Volume | 0.88 | 0.82 | 0.96 | 0.89 | 0.68 | 0.62 |
| | FA | 0.84 | 0.74 | 0.82 | 0.73 | 0.57 | 0.54 |
| Midbrain | Volume | 0.94 | 0.88 | 0.95 | 0.85 | 0.59 | 0.57 |
| | FA | 0.85 | 0.82 | 0.81 | 0.76 | 0.6 | 0.59 |
| Pons | Volume | 0.88 | 0,82 | 0.94 | 0.83 | 0.66 | 0,66 |
| | FA | 0.75 | 0.73 | 0.81 | 0.73 | 0.56 | 0.53 |
| Medulla oblongata | Volume | 0.69 | 0.64 | 0.81 | 0.72 | 0.67 | 0.63 |
| SN | NM volume | 1 | 1 | 1 | 1 | 0.96 | 0.86 |
| | NM signal | 0.89 | 0.86 | 0.76 | 0.76 | 0.94 | 0.88 |
| | FA | 0.96 | 0.97 | 0.93 | 0.95 | 0.65 | 0.62 |
| PPN | FA | 0.87 | 0.82 | 0.82 | 0.82 | 0.61 | 0.62 |
| Cuneiform | FA | 0.83 | 0.82 | 0.79 | 0.72 | 0.52 | 0.54 |
| | MD | 0.78 | 0.65 | 0.70 | 0.65 | 0.60 | 0.65 |
| LC | FA | 0.91 | 0.81 | 0.94 | 0.82 | 0.55 | 0.54 |
| | MD | 0.78 | 0.73 | 0.75 | 0.72 | 0.56 | 0.57 |
| Cerebellar cortex | FA | 0.81 | 0.76 | 0.67 | 0.64 | 0.61 | 0.62 |
| Cerebellar WM | FA | 0.71 | 0.67 | 0.72 | 0.71 | 0.56 | 0.58 |
| DN | FA | 0.88 | 0.79 | 0.86 | 0.85 | 0.57 | 0.54 |
| | MD | 0.66 | 0.64 | 0.77 | 0.8 | 0.57 | 0.53 |
| Superior frontal cortex | FA | 0.78 | 0.73 | 0.73 | 0.73 | 0.60 | 0.59 |
| Precentral cortex | FA | 0.75 | 0.64 | 0.76 | 0.64 | 0.54 | 0.53 |
| | MD | 0.77 | 0.72 | 0.76 | 0.73 | 0.56 | 0.57 |
| Anterior middle cingulate cortex | FA | 0.75 | 0.64 | 0.76 | 0.64 | 0.51 | 0.54 |
| | MD | 0.79 | 0.65 | 0.70 | 0.63 | 0.61 | 0.58 |
| Parieto-occipital cortex | FA | 0.75 | 0.72 | 0.69 | 0.63 | 0.59 | 0.61 |
| ST WM | FA | 0.89 | 0.82 | 0.91 | 0.82 | 0.56 | 0.57 |

*The variables allow the distinction between PSP and HC subjects with an AUC = 0.7;
volume in $mm^3$, MD in $\times 10^{-X}$ $mm^2.s^{-1}$.
CA, categorization accuracy; N, neuromelanin; ST, supratentorial; WM, white matter.

**TABLE 3.** Distribution of MRI changes versus previously published histological changes in PSP

| Region | Subregion | PSP | | PD |
|---|---|---|---|---|
| | | MRI | Histology* | MRI |
| Basal ganglia | Globus pallidus | +++ | +++ | + |
| | Caudate nucleus | ++ | ++ | + |
| | Putamen | ++ | ++ | + |
| | STN | +++ | +++ | + |
| | Thalamus | ++ | ++ | + |
| | Ch3 to 4 (nucleus basalis) | +++ | +++ | + |
| Brainstem | Midbrain | +++ | +++ | + |
| | SN | +++ | +++ | +++ |
| | PPN | +++ | +++ | ++ |
| | Cuneiform nucleus | + | + | ++ |
| | Pons | ++ | ++ | + |
| | LC | +++ | ++/+++ | 0 |
| | Medulla oblongata | + | ++ | ++ |
| Cerebellum | Cortex and white matter | ++ | + | 0 |
| Deep cerebellar nuclei | DN | ++ | ++/+++ | 0 |
| Cortex | Prefrontal cortex | + | + | + |
| | Parieto-occipital cortex | + | + | + |
| | Hippocampus | 0 | 0 | ++ |
| | Amygdala | 0 | 0 | ++ |
| | Temporal cortex | 0 | 0 | 0 |

The four lesion grades ranged from 0 to +++.
*Steele and colleagues, 1964; Dickson and colleagues, 2012.

well as for FA in the thalamus, SN, and DN. Additionally, a high categorization accuracy was observed for the midbrain surface, SCP diameter, midbrain-to-pons ratio, and MRPI.

## Grades of Change Computation

The structures with the highest grade (grade 3) were the SN, globus pallidus, midbrain, NBM (Ch3–4), LC, STN, and PPN. Grade 2 regions included the caudate nucleus, thalamus, pons, DN, and cerebellum. No significant changes were observed in the hippocampus, amygdala, or temporal cortex (Table 3; Fig. 1).

## MFA

Eigen values from the global PCA indicated that the first three factors explained 35.2%, 14.2%, and 8% of the total variance. The fourth and fifth factors explained only approximately 6% and 5% of the variance, respectively. We thus used a three-factor solution, which explained 61% of the variance. The first component was highly correlated with the globus pallidus, putamen, thalamus, cerebellar white matter, midbrain, pons, and STN, whereas the midbrain, pons, globus pallidus, thalamus, STN, NBM, cuneiform, and cerebellum cortex highly contributed to the variance of the second component. The SN, LC, caudate nucleus, and medulla oblongata contributed to both components, which suggested that alterations of these structures were more pronounced in PSP-RS than in PD, but were present in both diseases. An initial separation of the HC mean point (center of gravity) versus PD and PSP was observed along axis 1, and a second separation of the PD mean point versus PSP was observed along axis 2 (Fig. 2). This result suggested that the first component represented the disease (altered vs. nonaltered regions), whereas the second component suggested that individuals with PD and PSP were

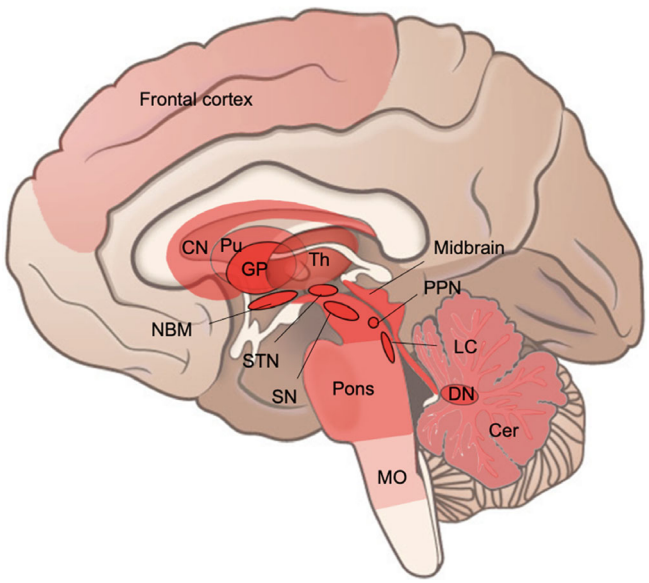


**FIG. 1.** Schematic representation of the severity of degeneration in PSP as detected by MRI. Results are shown according to the degeneration distribution in PSP using the 0 to 3 scale based on cut-off values and local extrema of ROC curves. Light red = grade 1; medium red = grade 2; dark red = grade 3. Cer, cerebellum; CN, cuneiform nucleus; GP, globus pallidus; MO, medulla oblongata; Pu, putamen; Th, thalamus.

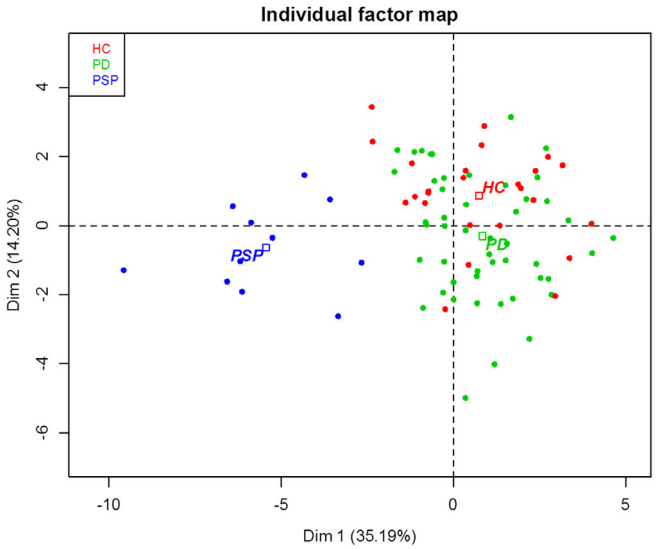


**FIG. 2.** Factorial analysis based on grades of change. Factorial analysis shows excellent separation between PSP and both HC and PD subjects, with the two dimensions explaining 35.2% and 14.2% of the total variance. Axis 1 separated HCs from PD and PSP subjects, while axis 2 separated PD from PSP subjects. Separation between PD and HC subjects was observed, with the mean points (square) being well separated, but there was a partial [Color figure can be viewed at wileyonlinelibrary.com]

differentiated by the set of brain regions highly correlated to the second axis.

### Logistic Regression

Logistic regression analysis showed that the best predictors for separating PSP-RS from HC subjects were the NM-based volume of the SN ($P < 0.001$); FA in the midbrain ($P = 0.004$); volumes of the midbrain ($P = 0.004$), entire brainstem ($P = 0.005$), globus pallidus ($P = 0.01$), and putamen (0.02); and FA in the LC ($P = 0.003$). The best predictors for separating PSP-RS from PD subjects were (in descending order) the NM-based volume of the SN ($P < 0.001$), FA in the pons ($P < 0.002$), midbrain volume ($P = 0.004$), volume of the globus pallidus ($P = 0.006$), and FA in the NBM ($P = 0.007$). The best predictors for separating HC from PD subjects were the NM-based SN volume ($P < 0.001$), NM-based SN signal ($P = 0.01$), SN FA ($P = 0.001$) and putamen FA ($P = 0.02$).

## Discussion

Our results showed that multimodal quantitative MRI biomarkers allowed direct noninvasive evaluation of the brain lesions in PSP not only in relatively large brain regions, such as the thalamus and midbrain, as reported previously, but also, for the first time, in small nuclei and the basal forebrain (especially the STN, cuneiform nucleus, pedunculopontine, and NBM). The distribution of affected areas and the relative importance of regional changes, analyzed using volumetric MRI, DTI, and neuromelanin sensitivity, was consistent with those previously reported in pathology studies.[1,6] As expected, the precise patterns of change and the severity of the lesions differed between PSP and PD subjects. These results suggest that an accurate assessment and staging of brain lesions in PSP could be obtained using multimodal MRI, which may help in the clinical diagnosis of the disease.

The clinical diagnostic criteria of the NINDS and the Society for PSP (NINDS-SPSP) have demonstrated a high positive predictive value for PSP diagnosis, but have variable sensitivity, particularly during the early course of the disease,[21] because oculomotor features may develop late or never.[22] More recently, new criteria have been proposed by the MDS, including oculomotor dysfunction, postural instability, akinesia, and cognitive dysfunction.[2] Nevertheless, to date, the diagnosis of "definite PSP" relies on the postmortem neuropathological examination.[8,23]

Pathologically, PSP is a tauopathy characterized by the presence of abnormally hyperphosphorylated tau-positive neurofibrillary tangles, neuropil threads, and inclusions in astrocytes and oligodendroglia in several cortical and subcortical structures.[1,6,7,23] Structures that are mostly affected in pathological studies include the globus pallidus, STN, SN, and LC, followed by the NBM, oculomotor complex, superior colliculus, periaqueductal gray matter, PPN, cuneiform nuclei, and DN.[1,6] The cortex, particularly the frontal lobes and the premotor cortex, was also found to be involved.[8] The topography of pathological lesions varied according to the clinical phenotype of the disease.[3] With multimodal MRI, we were able to detect brain lesions in all structures that we studied wherein pathological changes have been described, including, for the first time, the NBM, STN, PPN, and cuneiform nucleus. Moreover, cortical changes were not found in regions that are usually spared in the disease, such as the temporal cortex, amygdala, and hippocampus. The magnitude of changes in these regions mirrored that reported in pathological studies; the regions with the most significant MRI involvement were those with the greatest pathological involvement, with a similar ranking of changes. The superior colliculus and periaqueductal gray matter were not studied separately herein because of the lack of available masks of these structures, but were part of the midbrain region.

Imaging has already been used to detect brain changes in patients with PSP and helped in the positive and differential diagnosis of the disease. Structural imaging has been the most commonly used technique to date.[24] Brainstem changes were consistently found in patients with PSP in both imaging and pathological studies, with the midbrain being the most involved area. Visual evaluation of midbrain atrophy in patients with PSP showed a characteristic shape on midline T1-w sagittal sections, visible as a flat or concave aspect of the normal convex profile of its superior border.[9] By semiquantitative evaluation, brainstem atrophy has been quantified using indices such as the midbrain/pons ratio[9-11,25]; the anteroposterior midbrain

diameter; the midbrain, colliculus, and pontine tegmentum diameters or surfaces[9,26]; and the MRPI.[27] Gray and white matter reductions in patients with PSP were also constantly reported in the midbrain, including the SCP and the colliculus area, as well as to a lesser degree and more inconsistently in the pons, using voxel-based morphometry (VBM).[14,28] Our results are in line with these studies, given that midbrain atrophy exhibited an excellent categorization accuracy of separating PSP patients from both PD and HC subjects, and pons atrophy exhibited a lesser performance. FA also showed high categorization accuracy, given that it was decreased in the midbrain and pons in patients with PSP, allowing the differentiation from HC and PD subjects. The categorization accuracy of FA was lower in the pons than in the midbrain, in agreement with previous studies.[13,14,29]

Changes in the medulla oblongata in patients with PSP were variable in previous studies. In pathological studies, neurodegeneration in this area ranged from mild to moderate.[23] In imaging studies, a reduced medulla oblongata volume was inconsistently observed in some studies.[26,30] Here, we found mild changes in the medulla oblongata in patients with PSP, suggesting that although MRI was able to detect changes in this area, these changes had a low categorization accuracy.

Extensive alterations were observed in the SN and LC, in line with previous pathological studies.[1,6,23] In the SN, the categorization accuracy of both NM-sensitive imaging and FA was good to excellent for differentiating patients with PSP from both HC and PD subjects. Previous studies have reported that variable NM-positive abnormalities in the SNs of patients with PSP were found to be less than,[31] greater than,[32] or similar to those in PD patients.[33] The disagreement between studies concerning the extent of changes may be related to the variability of the disease or the measurement techniques and needs to be investigated in a larger group of patients. In our study, the NM-sensitive volume was lower in PSP subjects than in PD subjects, suggesting that NM-sensitive imaging may contribute to distinguishing PSP from PD. The LC was also altered in subjects with PSP, confirming the results of a previous imaging study,[31] to a greater extent than that in PD patients, as reported previously.[17]

We found changes in the PPN and cuneiform nucleus to be in line with those described in previous pathological studies on PSP.[1,34] Previous MRI studies have reported a decrease in functional connectivity in the PPN in patients with PD,[35] whereas in those with PSP, PPN network degeneration was explored using [18F]-FDG-PET.[36] To our knowledge, this study is the first anatomical MRI analysis of these structures in PSP.

FA was reduced in the DN in accord with previous pathological studies.[1,6] Lesions in the DN may result in marked atrophy of the SCP.[6] Patients with PSP also presented cerebellar alterations, as previous imaging and pathological studies have reported.[11]

Pathological studies have shown that the basal ganglia are among the most affected structures in patients with PSP, with the globus pallidus[24,37] and the STN being more affected than the striatum.[23] Here, we also found greater volume loss for the globus pallidus than for the putamen, which allowed us to distinguish PSP subjects from PD and HC subjects. Although to a lesser extent, marked striatal volume loss was observed in both the putamen and the caudate nucleus, in line with previous studies.[38] Changes were also reported in the basal ganglia using diffusion imaging, with significant alterations being observed in the globus pallidus and, to a lesser extent, the striatum.[12,14,29,39] It should be noted that the striatum cannot be considered a normal region in patients with PSP, although it is affected to a lesser extent in these patients than in those with diseases for which a differential diagnosis is difficult, such as MSA. However, the separate categorization performances of the FA decrease and MD increase in these structures were low. In future studies, it would be interesting to more specifically investigate changes in the internal and external segments of the globus pallidus and subregions of the putamen and calculate other promising metrics, such as diffusion-based free water, that have proven to be more effective than the DTI metrics in the SN.[40] Although pathologically the STN was previously shown to be one of the most affected structures in PSP,[41] no structural changes or Lewy pathologies have been reported in the STN.[42] Our results are in line with previous studies showing volume decreases in PSP, but not in PD subjects. Given the small size of the structure, only a few MRI studies have investigated the STN volume in humans, mostly using 7T MRI in healthy volunteers, finding a correlation between volume reduction and age.[43,44] In PSP, elevated free water diffusion,[39] increased iron content using R2* relaxometry,[45] and elevated tau tracer binding using PET[46] were reported. In PD, the MRI results were discordant, showing no changes[47] or a reduction in STN volume.[48] It should be noted that these studies were performed at 3T, where the spatial resolution was not as high as that attained at 7T, with a higher risk of large partial volume effects. In this study, 7T measurements allowed for precise analysis of the STN, even if the variability in STN volume in HCs was relatively high, probably attributable to the small size of the structure. Although 7T measurements are not widespread in clinical practice, the classification and distinction of PD and PSP patients remain good when only 3T-related measurements are retained in the model. However, given its high spatial resolution, 7T imaging remains of high interest for the analysis of small structures, such as the STN.

MRI changes were found in the thalamus of patients with PSP, in accord with pathological studies, with both volume and FA having good categorization accuracies. Previous VBM studies have reported gray and white matter reductions in the thalamus, particularly in

pulvinar, dorsomedial, and anterior nuclei.[14,28] Diffusion changes have been inconsistently reported.[12,29,39]

Patients with PSP have been shown to exhibit cortical atrophy typically involving the frontal lobes. VBM studies on PSP have reported gray and white matter reductions in the frontal cortex, particularly in the premotor cortex, insula, hippocampal, and parahippocampal regions.[24,28] Using diffusion imaging, changes were reported in the precentral white matter[14] and more variably in the white matter of the cerebral hemispheres predominating the frontal lobes.[28,30] In our study, the diffusion changes mostly concerned the prefrontal cortex and parieto-occipital cortex, in line with previous pathological analyses.[1,6]

Our study has several limitations. First, the number of subjects with PSP included in the study was low, and the results need to be confirmed in a larger group of subjects. However, despite the small number of subjects, the population appeared homogeneous, with the same regions being affected in all subjects and corresponding to the results of histological studies.[1,6] In addition, the volume declines observed in our study were generally of the same order of magnitude as those observed previously (cerebellum, frontal lobe, or basal ganglia).[38] Second, the diagnosis of PSP was made clinically using international standards, although the definitive diagnosis is based on pathological examination. However, the results suggested that multimodal MRI was able to capture changes at multiple levels of the brain in regions known to be affected in PSP. Third, we focused on the classical Richardson form of PSP. This proof-of-concept study investigated the feasibility of using MRI analysis to detect and grade changes with comparable results to histological analysis, for most areas affected by the disease including the smallest regions that are thus far unexplored. Considering these results, the study of patients with PSP variants other than PSP-RS appears promising, but this remains to be determined. Fourth, the mean age of our patients was relatively low, and it would be interesting to determine whether our results are also valid for older patients with possible comorbidities. Finally, some new promising biomarkers, such as quantitative susceptibility mapping, were not included in the present study. Future cohort studies should be planned to explore these biomarkers.

In summary, quantitative MRI biomarkers allowed the in vivo detection of brain damage in patients with PSP in not only large basal ganglia regions, as reported previously, but also in small brainstem and basal forebrain structures, and these results are in excellent agreement with the known topography of damage reported in previous pathological studies. Moreover, these biomarkers exhibited excellent categorization accuracies for differentiating PSP from PD patients. ■

**Acknowledgments:** We thank Mr Alain Mallart for his unrestricted support for research on Parkinson's disease.

## References


1. Steele JC, Richardson JC, Olszewski J. Progressive supranuclear palsy. A heterogeneous degeneration involving the brain stem, basal ganglia ans cerebellum with vertical gaze and pseudobulbar palsy, nuchal dystonia and dementia. Arch Neurol 1964;10:333–359.
2. Höglinger GU, Respondek G, Stamelou M, et al. Clinical diagnosis of progressive supranuclear palsy: the Movement Disorder Society criteria. Mov Disord 2017;32:853–864.
3. Boxer AL, Yu JT, Golbe LI, Litvan I, Lang AE, Höglinger GU. Advances in progressive supranuclear palsy: new diagnostic criteria, biomarkers, and therapeutic approaches. Lancet Neurol 2017;16:552–563.
4. Litvan I, Agid Y, Calne D, et al. Clinical research criteria for the diagnosis of progressive supranuclear palsy (Steele-Richardson-Olszewski syndrome): report of the NINDS-SPSP international workshop. Neurology 1996;47:1–9.
5. Respondek G, Roeber S, Kretzschmar H, et al. Accuracy of the National Institute for Neurological Disorders and Stroke/Society for Progressive Supranuclear Palsy and neuroprotection and natural history in Parkinson plus syndromes criteria for the diagnosis of progressive supranuclear palsy. Mov Disord 2013;28:504–509.
6. Dickson DW. Parkinson's disease and parkinsonism: neuropathology. Cold Spring Harb Perspect Med 2012;2:a009258.
7. Rösler TW, Tayaranian Marvian A, Brendel M, et al. Four-repeat tauopathies. Prog Neurobiol 2019;180:101644.
8. Verny M, Duyckaerts C, Agid Y, Hauw JJ. The significance of cortical pathology in progressive supranuclear palsy. Clinico-pathological data in 10 cases. Brain J Neurol 1996;119(Pt 4):1123–1136.
9. Righini A, Antonini A, De Notaris R, et al. MR imaging of the superior profile of the midbrain: differential diagnosis between progressive supranuclear palsy and Parkinson disease. Am J Neuroradiol 2004;25:927–932.
10. Oba H, Yagishita A, Terada H, et al. New and reliable MRI diagnosis for progressive supranuclear palsy. Neurology 2005;64:2050–2055.
11. Paviour DC, Price SL, Jahanshahi M, Lees AJ, Fox NC. Longitudinal MRI in progressive supranuclear palsy and multiple system atrophy: rates and regions of atrophy. Brain J Neurol 2006;129:1040–1049.
12. Seppi K, Schocke MFH, Esterhammer R, et al. Diffusion-weighted imaging discriminates progressive supranuclear palsy from PD, but not from the parkinson variant of multiple system atrophy. Neurology 2003;60:922–927.
13. Blain CRV, Barker GJ, Jarosz JM, et al. Measuring brain stem and cerebellar damage in parkinsonian syndromes using diffusion tensor MRI. Neurology 2006;67:2199–2205.
14. Lehéricy S, Hartmann A, Lannuzel A, et al. Magnetic resonance imaging lesion pattern in Guadeloupean parkinsonism is distinct from progressive supranuclear palsy. Brain J Neurol 2010;133:2410–2425.
15. Whitwell JL, Avula R, Master A, et al. Disrupted thalamocortical connectivity in PSP: a resting-state fMRI, DTI, and VBM study. Parkinsonism Relat Disord 2011;17:599–605.
16. Pyatigorskaya N, Magnin B, Mongin M, et al. Comparative study of MRI biomarkers in the substantia nigra to discriminate idiopathic Parkinson disease. Am J Neuroradiol 2018;39:1460–1467.
17. García-Lorenzo D, Longo-Dos Santos C, Ewenczyk C, et al. The coeruleus/subcoeruleus complex in rapid eye movement sleep behaviour disorders in Parkinson's disease. Brain J Neurol 2013;136:2120–2129.
18. Bardinet E, Bhattacharjee M, Dormont D, et al. A three-dimensional histological atlas of the human basal ganglia. II. Atlas deformation strategy and evaluation in deep brain stimulation for Parkinson disease. J Neurosurg 2009;110:208–219.
19. Gargouri F, Gallea C, Mongin M, et al. Multimodal magnetic resonance imaging investigation of basal forebrain damage and cognitive deficits in Parkinson's disease. Mov Disord 2019;34:516–525.
20. Schwarz ST, Rittman T, Gontu V, Morgan PS, Bajaj N, Auer DP. T1-weighted MRI shows stage-dependent substantia nigra signal loss in Parkinson's disease. Mov Disord 2011;26:1633–1638.
21. Osaki Y, Ben-Shlomo Y, Lees AJ, et al. Accuracy of clinical diagnosis of progressive supranuclear palsy. Mov Disord 2004;19:181–189.

22. Collins SJ, Ahlskog JE, Parisi JE, Maraganore DM. Progressive supranuclear palsy: neuropathologically based diagnostic clinical criteria. J Neurol Neurosurg Psychiatry 1995;58:167–173.
23. Hauw JJ, Daniel SE, Dickson D, et al. Preliminary NINDS neuropathologic criteria for Steele-Richardson-Olszewski syndrome (progressive supranuclear palsy). Neurology 1994;44:2015–2019.
24. Whitwell JL, Höglinger GU, Antonini A, et al. Radiological biomarkers for diagnosis in PSP: where are we and where do we need to be? Mov Disord 2017;32:955–971.
25. Massey LA, Jäger HR, Paviour DC, et al. The midbrain to pons ratio: a simple and specific MRI sign of progressive supranuclear palsy. Neurology 2013;80:1856–1861.
26. Schrag A, Good CD, Miszkiel K, et al. Differentiation of atypical parkinsonian syndromes with routine MRI. Neurology 2000;54: 697–702.
27. Morelli M, Arabia G, Messina D, et al. Effect of aging on magnetic resonance measures differentiating progressive supranuclear palsy from Parkinson's disease. Mov Disord 2014;29:488–495.
28. Padovani A, Borroni B, Brambati SM, et al. Diffusion tensor imaging and voxel based morphometry study in early progressive supranuclear palsy. J Neurol Neurosurg Psychiatry 2006;77: 457–463.
29. Nicoletti G, Lodi R, Condino F, et al. Apparent diffusion coefficient measurements of the middle cerebellar peduncle differentiate the Parkinson variant of MSA from Parkinson's disease and progressive supranuclear palsy. Brain J Neurol 2006;129:2679–2687.
30. Höglinger GU, Schöpe J, Stamelou M, et al. Longitudinal magnetic resonance imaging in progressive supranuclear palsy: a new combined score for clinical trials. Mov Disord 2017;32:842–852.
31. Ohtsuka C, Sasaki M, Konno K, et al. Differentiation of early-stage parkinsonisms using neuromelanin-sensitive magnetic resonance imaging. Parkinsonism Relat Disord 2014;20:755–760.
32. Taniguchi D, Hatano T, Kamagata K, et al. Neuromelanin imaging and midbrain volumetry in progressive supranuclear palsy and Parkinson's disease. Mov Disord 2018;33:1488–1492.
33. Kashihara K, Shinya T, Higaki F. Reduction of neuromelanin-positive nigral volume in patients with MSA, PSP and CBD. Intern Med Tokyo Jpn 2011;50:1683–1687.
34. Williams DR, Lees AJ. Progressive supranuclear palsy: clinicopathological concepts and diagnostic challenges. Lancet Neurol 2009;8:270–279.
35. Ewenczyk C, Mesmoudi S, Gallea C, et al. Antisaccades in Parkinson disease: a new marker of postural control? Neurology 2017;88:853–861.
36. Zwergal A, la Fougère C, Lorenzl S, et al. Functional disturbance of the locomotor network in progressive supranuclear palsy. Neurology 2013;80:634–641.
37. Massey LA, Micallef C, Paviour DC, et al. Conventional magnetic resonance imaging in confirmed progressive supranuclear palsy and multiple system atrophy. Mov Disord 2012;27:1754–1762.
38. Huppertz H-J, Möller L, Südmeyer M, et al. Differentiation of neurodegenerative parkinsonian syndromes by volumetric magnetic resonance imaging analysis and support vector machine classification. Mov Disord 2016;31:1506–1517.
39. Planetta PJ, Ofori E, Pasternak O, et al. Free-water imaging in Parkinson's disease and atypical parkinsonism. Brain J Neurol 2016; 139:495–508.
40. Ofori E, Krismer F, Burciu RG, et al. Free water improves detection of changes in the substantia nigra in parkinsonism: A multisite study. Mov Disord 2017;32:1457–1464.
41. Dickson DW, Ahmed Z, Algom AA, Tsuboi Y, Josephs KA. Neuropathology of variants of progressive supranuclear palsy. Curr Opin Neurol 2010;23:394–400.
42. Braak H, Del Tredici K, Rüb U, de Vos RAI, Jansen Steur ENH, Braak E. Staging of brain pathology related to sporadic Parkinson's disease. Neurobiol Aging 2003;24:197–211.
43. Plantinga BR, Temel Y, Duchin Y, et al. Individualized parcellation of the subthalamic nucleus in patients with Parkinson's disease with 7T MRI. NeuroImage 2018;168:403–411.
44. Zwirner J, Möbius D, Bechmann I, et al. Subthalamic nucleus volumes are highly consistent but decrease age-dependently-a combined magnetic resonance imaging and stereology approach in humans. Hum Brain Mapp 2017;38:909–922.
45. Lee SH, Lyoo CH, Ahn SJ, Rinne JO, Lee MS. Brain regional iron contents in progressive supranuclear palsy. Parkinsonism Relat Disord 2017;45:28–32.
46. Schonhaut DR, McMillan CT, Spina S, et al. 18 F-flortaucipir tau positron emission tomography distinguishes established progressive supranuclear palsy from controls and Parkinson disease: a multicenter study. Ann Neurol 2017;82:622–634.
47. Alkemade A, de Hollander G, Keuken MC, et al. Comparison of T2*-weighted and QSM contrasts in Parkinson's disease to visualize the STN with MRI. PLoS One 2017;12:e0176130.
48. Colpan ME, Slavin KV. Subthalamic and red nucleus volumes in patients with Parkinson's disease: do they change with disease progression? Parkinsonism Relat Disord 2010;16:398–403.

## Supporting Data

Additional Supporting Information may be found in the online version of this article at the publisher's web-site.